Solar Energy 185 (2019) 222–234

Contents lists available at ScienceDirect

Solar Energy

journal homepage: www.elsevier.com/locate/solener

Thermal stratification in a cylindrical tank due to heat losses while in standby mode

Yakai Bai[a,b,c,d], Ming Yang[a,b,c,d,e], Zhifeng Wang[a,b,c,d,e,*], Xiaoxia Li[a,b,d,f], Longfei Chen[a,f]

[a] Key Laboratory of Solar Thermal Energy and Photovoltaic Systems, Chinese Academy of Sciences, Beijing 100190, China
[b] Institute of Electrical Engineering, Chinese Academy of Sciences, Beijing 100190, China
[c] University of Chinese Academy of Sciences, Beijing 100049, China
[d] Beijing Engineering Research Center of Solar Thermal Power, Beijing 100190, China
[e] Guangdong Fivestar Solar Energy Co., Ltd, Dongguan, Guangdong 523058, China
[f] Lanzhou University of Technology, Lanzhou 730050, China

ARTICLE INFO

Keywords:
Heat loss
Thermal stratification
CFD
Energy storage
Cylindrical tank

ABSTRACT

The liquid in an energy storage tank will become thermally stratified during cooling of the tank when the tank is not charging or discharging. This process is studied here experimentally and numerically. A two-dimensional model validated against experimental data is used to study the thermal stratification mechanisms during cooling. The results show that natural convection mainly along the upper side of the cylindrical tank creates a boundary layer along the sidewall that drives cooled water down the side. The two-dimensional analysis is used to create a one-dimensional model for the cooling process that is validated against the experimental data. The one-dimensional model is then used to investigate the influence of the height to diameter aspect ratio on the cooling process. A tank with an aspect ratio of 1:1 has the highest energy efficiency, highest exergy efficiency, and lowest entropy generation during cooling. Further study shows that when the aspect ratio is smaller than 3, the thermal stratification increases greatly with increasing aspect ratio. Aspect ratios bigger than 3 have little influence on the thermal stratification.

1. Introduction

Energy storage is an important issue in solar engineering systems (Zhang et al., 2016). Most previous studies have focused on charging and discharging of a storage tank (Avallone et al., 2016; Wang et al., 2017a, 2017b; Yaïci et al., 2013), but the cooling during the night is more important. This cooling will cause thermal stratification in the tank which will influence the solar collector system performance (Chang et al., 2017; Yaïci et al., 2013). Thus, a study on the tank cooling without charging and discharging is important.

Some studies of the tank charging and discharging processes have presented simple models for the tank fluid that were validated with charging and discharging experiments (Baeten et al., 2016). However, most studies in this area have used CFD simulations (Cabelli, 1977) or experiments (Padilha, 1983). They have focused on enhancing the thermal stratification in the water storage tank by proper selection of the inlet and outlet locations in the tank (Alizadeh, 1999) or by placing flat plates or obstacles inside the water storage tank (Bouhal et al., 2017; Erdemir and Altuntop, 2016; Wang et al., 2017a, 2017b). The charging and discharging processes have been characterized by various dimensionless numbers such as the Richardson number, Stratification number, and MIX number to evaluate the thermal stratification in the tank (Castell et al., 2010). Other parameter like the thermocline thickness have also been used (Chang et al., 2016) but none of these parameters are suitable for describing cooling of a storage tank without charging or discharging.

Studies of storage tank cooling have computational fluid dynamics (CFD) models to investigate the thermal stratification mechanisms. Oliveski et al. have done many experiments and simulations of tank cooling with oil or water in the tank and presented correlations of the natural convection heat transfer coefficient in a cylindrical tank (De Césaro Oliveski, 2013; De Césaro Oliveski et al., 2003; Oliveski et al., 2003, 2005; Rodríguez et al., 2009). However, the Rayleigh number definition was modified to differ from that for large-scale natural convection, so these results cannot be easily compared with others. Yang et al. also studied the heat loss process with a comparison of the

* Corresponding author at: Key Laboratory of Solar Thermal Energy and Photovoltaic Systems, Chinese Academy of Sciences, Beijing 100190, China.
E-mail address: zhifeng@vip.sina.com (Z. Wang).

https://doi.org/10.1016/j.solener.2018.12.063
Received 25 February 2018; Received in revised form 25 November 2018; Accepted 24 December 2018
Available online 24 April 2019
0038-092X/

Nomenclature

0	initial state
c_p	specific heat at constant pressure in the fluid region,J·kg $^{-1}$·K $^{-1}$
D	tank diameter, m
E	internal energy, J
e	internal energy per unit mass,J·kg $^{-1}$
Ex	internal exergy, J
ex	internal exergy per unit mass,J·kg $^{-1}$
g	gravitational acceleration, m·s^{-2}
Gr	Grashof number,$Gr = g\beta\Delta TL_{ref}{}^3/\upsilon^2$
h	convection coefficient, W·m^{-2}·K^{-1}
H	tank height, m
l	reference length, m
M	mass of each segment, kg
Nu	Nusselt number,$Nu = hl/\lambda$
p	pressure, Pa
Pr	Prandtl number,$Pr = \upsilon/\alpha$
q	heat transfer, W
Ra	Rayleigh number,$Ra = PrGr$
r	radial position, m
U	heat loss coefficient,W·m $^{-2}$·K^{-1}
u	axial velocity in the fluid, m·s^{-1}
V	tank volume, m^3
v	radial fluid velocity, m·s^{-1}
S_{gen}	entropy generation during cooling, J·K^{-1}
$\dot{S}_{gen}$	entropy generation rate,J·s $^{-1}$·K $^{-1}$
T	fluid temperature, K
t	time, s
z	axial position, m

Subscripts

$-$	average
c	cooled water
env	ambient
i	ith segment
ins	insulation
max	maximum
min	minimum
s	side wall
t	top wall
w	wall

Greek

ρ	density,kg·m $^{-3}$
μ	dynamic viscosity of the fluid,Pa·s
β	thermal expansion coefficient of the fluid region, K^{-1}
δ	insulation thickness, m
η_1	thermal energy storage efficiency, %
η_2	thermal exergy storage efficiency, %
Δz	segment thickness, m

influence of the tank shape on the thermal stratification using the maximum temperature difference in the tank to evaluate the thermal stratification effect (Yang et al., 2016). Lin et al. numerically investigated tank cooling from the side wall which created thermal stratification even though the top and bottom of the tank were adiabatic (Lin and Armfield, 1999). A scaling analysis was used to characterize the development of the vertical thermal boundary layer along the side wall and the stratification in the cylindrical tank. Kursun et al. studied the influence of rectangular hot water tank position and aspect ratio on the thermal stratification and showed that the highest temperature difference in the hot water tank occurred for a side angle of $\alpha = 45°$ and an aspect ratio of D/H = 0.5, but they did not consider tanks with D/H smaller than 0.5 (Kurşun and Ökten, 2018). They have also studied the thermal stratification in cylindrical and rectangular hot water tanks with truncated cones and pyramid shaped insulation (Kurşun, 2018). Papanicolaou et al. studied tank heating from the side wall at high Rayleigh numbers (Papanicolaou and Belessiotis, 2002). The results showed that with an aspect ratio of H/D = 1 and Prandtl numbers ranging from 2.965 to 5.388, the laminar regime was obtained for Rayleigh numbers (based on the tank length) up to $Ra = 5 \times 10^{13}$ with turbulent flow for $Ra > 5 \times 10^{13}$. Karatas and Derbentli studied the natural convection of air in a cavity and presented correlations for the natural convection heat transfer coefficient for various aspect ratios (Karatas and Derbentli, 2017).

CFD calculations are very time-consuming and not practical for long-term simulations. Thus, a simplified one-dimensional model is needed to simplify the models. A multinode model was validated with experimental results by Alizadeh (1999) and has been incorporated into TRNSYS (Thornton et al., 2010; Klein, 1988) for long-term calculations of the thermal conditions in storage tanks. The disadvantage of this simplified model is that it does not include buoyancy-driven flow that results from heat losses which leads to physically inconsistent results

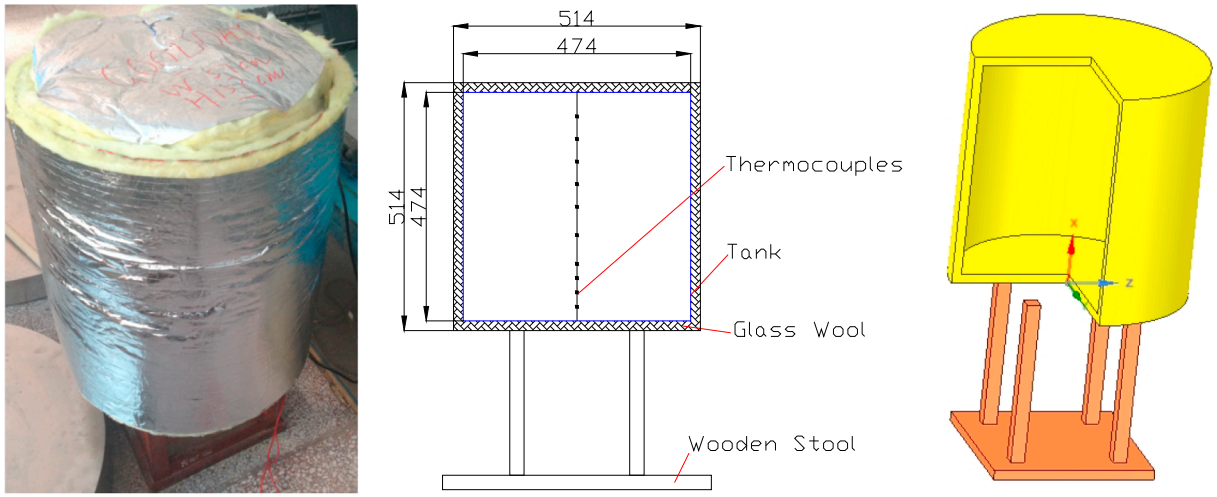

Fig. 1. Experiment tank and temperature measurement points.

(De Césaro Oliveski et al., 2003; Fan and Furbo, 2012; Fan et al., 2015). This model was improved by Powell and Edgar (Powell and Edgar, 2013) with an adaptive grid method to make it faster and also fixed the physically inconsistencies. Cruickshank and Harrison (2010) modeled the heat loss from a storage tank in another way with different heat loss coefficients along the tank height measured in experiments that caused thermal stratification. The model worked well but did not have a clear physical basis and was hard to apply to designing storage tanks. De Césaro Oliveski et al. (2003) used the multinode with inverse method (MI, Klein (1988)) and the multinode with mean method (MM, Franke (1997)) to simulate the heat losses with the results validated against CFD results. These methods all fixed the physically inconsistency problem. However, they neglected the thermal stratification caused by natural convection near the side wall which is analyzed in this paper. (Fan and Furbo, 2012; Fan et al., 2015) presented a model to predict the temperature distribution during the heat loss process based on fitting parameters from CFD simulations. The thermal stratification caused by heat losses from the side and the top wall were both taken into account, but the correlation was quite complex and the method has not been validated. The maximum temperature difference in the tank and exergy efficiency have been most commonly used to evaluate the cooling effects in storage tanks.

This paper analyzes the thermal stratification mechanisms in a cylindrical water storage tank to develop a simple but effective way to model the heat loss effects in a storage tank. First, the thermal flow characteristics during the cooling are studied experimentally and with a two-dimensional analysis. These give dimensionless correlations for the Nusselt number along the side and top walls. Then, the two-dimensional model results and the thermal stratification mechanisms in the tank are used to develop a computational model that takes into account the natural convection near the side wall and the top wall that is validated with experimental data. Finally, this model is used to study the heat losses from cylindrical water tanks with various height to diameter ratios.

2. Experimental apparatus

The experiments were designed to validate the mathematical model given in Section 3. Fig. 1 shows a diagram of the experimental apparatus. The tests were conducted on a vertical cylindrical tank that was 474 mm tall, had an inner radius of 474 mm, and a wall thickness of 1 mm. The tank was fabricated from stainless steel 304. The tank was covered with a 20 mm thick layer of glass wool. A wooden base was used to support the tank.

The temperatures were measured at 11 points with the data recorded in a computer once a minute through a data acquisition card. The temperatures were measured by 1 mm diameter T-type thermocouples. An uncertainty analysis considering the temperature measurement error, time effect, and data acquisition card gave a mean uncertainty of ± 0.1 °C evaluated according to the method prescribed by Chang et al. (2017). Fig. 1 shows the distribution of the measuring points in the experiment. The distances of the thermocouples from the bottom are listed in Table 1.

An 4 kW electrical resistance heater was used to heat the water in the tank. After heating, the heater was pulled out of the tank. During the experiments, the tank was allowed to cool starting from 99.5 °C. The ambient temperature was about 26 °C and did not vary greatly during the experiments.

3. Thermal flow characteristics during the cooling process

A CFD model was used to study the thermal flow characteristics during the cooling with the results used to improve the one-dimensional model. For the case studied in this work, the Rayleigh number at the beginning based on the tank height was about 2×10^{10}. Many authors have used laminar flow simulations to model natural convection in tanks (Fan and Furbo, 2012; Zhang et al., 2016) and the current conditions were also assumed to be laminar flow (Lin and Armfield, 1999; Papanicolaou and Belessiotis, 2002). In addition, the flow in the vertical tank was assumed to be axisymmetric; thus, a two-dimensional laminar model was used.

3.1. Mathematical model

3.1.1. Governing equations

Continuity equation:

$$\frac{\partial \rho}{\partial t} + \frac{\partial (\rho u)}{\partial z} + \frac{1}{r}\frac{\partial (\rho r v)}{\partial r} = 0 \tag{1}$$

Momentum equations:

$$\frac{\partial (\rho u)}{\partial t} + \frac{\partial (\rho u u)}{\partial z} + \frac{\partial (\rho v u)}{\partial r} = -\frac{\partial p}{\partial z} + \mu\left(\frac{\partial^2 u}{\partial z^2} + \frac{1}{r}\frac{\partial u}{\partial r} + \frac{\partial^2 u}{\partial r^2}\right) + \rho g$$

$$\frac{\partial (\rho v)}{\partial t} + \frac{\partial (\rho u v)}{\partial z} + \frac{\partial (\rho v v)}{\partial r} = -\frac{\partial p}{\partial z} + \mu\left(\frac{\partial^2 u}{\partial z^2} + \frac{1}{r}\frac{\partial v}{\partial r} + \frac{\partial^2 v}{\partial r^2} - \frac{v}{r^2}\right) \tag{2}$$

Energy equation:

$$c_p\left[\frac{\partial (\rho T)}{\partial t} + \frac{\partial (\rho u T)}{\partial z} + \frac{\partial (\rho v T)}{\partial r}\right] = \lambda\left(\frac{\partial^2 T}{\partial z^2} + \frac{1}{r}\frac{\partial T}{\partial r} + \frac{\partial^2 T}{\partial r^2}\right) \tag{3}$$

$$\rho = 863 + 1.21T - 0.00257T^2;\ \mu = 0.0007\left(\frac{T}{315}\right)^{-5.5};\ \lambda = 0.375 + 8.84 \times 10^{-4}T \tag{4}$$

A constant specific heat of water of 4180 J/kg/K was used in the CFD model. The energy equation for the insulation was:

$$c_{p,ins}\left[\frac{\partial (\rho_{ins} T_{ins})}{\partial t}\right] = \lambda_{ins}\left(\frac{\partial^2 T_{ins}}{\partial z^2} + \frac{1}{r}\frac{\partial T_{ins}}{\partial r} + \frac{\partial^2 T_{ins}}{\partial r^2}\right) \tag{5}$$

3.1.2. Boundary conditions

The initial conditions were zero velocities and isothermal temperature (T_0 = 99.5 °C).

$$u = 0;\ v = 0;\ T = T_0;\ T_{ins} = T_{env}; \tag{6}$$

The boundary condition for the energy equation along the axis of the water region was:

$$u = 0;\ v = 0;\ \frac{\partial T}{\partial r} = 0; \tag{7}$$

The boundary condition for the insulation region along the axis was:

$$\frac{\partial T_{ins}}{\partial r} = 0 \tag{8}$$

The no-slip boundary condition and the coupled thermal boundary condition were imposed on the fluid wall:

$$u = 0;\ v = 0;\ T = T_{ins},\ q = q_{ins} \tag{9}$$

Table 1
Thermocouples locations from the tank bottom.

Thermocouples	Height/m
1	0.424
2	0.371
3	0.318
4	0.265
5	0.212
6	0.159
7	0.106
8	0.080
9	0.053
10	0.027
11	0.000

The boundary conditions along the top, side, and bottom walls of the thermal insulation layer were modeled with an external convection coefficient. The sides were:

$$-\lambda_{ins}\frac{\partial T_{ins}}{\partial r} = h_{env}(T_{ins} - T_{env}) \quad (10)$$

The top and bottom walls of the external surface were:

$$-\lambda_{ins}\frac{\partial T_{ins}}{\partial z} = h_{env}(T_{ins} - T_{env}) \quad (11)$$

Lin et al. used h_{env} set to 2 W/m^2/K, but this is much lower than that measured in this work (Lin and Armfield, 1999). Therefore, the natural convection coefficient on the air side was modeled using:

$$\bar{h}_{env} = 0.051(\bar{T} - T_{env}) + 3.092 \quad (12)$$

In the case studied here, the insulation outer surface temperature was less than 35 °C, so h_{env} = 3.6 W/m^2/K was used.

3.2. Numerical verification and model validation

3.2.1. Numerical verification

The PRESTO was used to model the pressure terms with the second-order upwind method used to model the convection terms. The SIMPLE algorithm was used for the pressure-velocity coupling. The calculation was considered convergent if the scaled residual for the momentum equations were all less than 10^{-3}, that of the energy equation was less than 10^{-6} and that of the continuity equation was less than 10^{-3} or the normalized mass flow residue for any grid volume was less than 10^{-4} kg s^{-1}. Four types of mesh are studied to validate the mesh independence with the detailed mesh information listed in Table 2.

Fig. 2 shows the temperature distributions in the fluid region for the various grid schemes. The distributions in the axial direction at r = 0 m and in the radial direction at h = 0.257 m are shown in Table 2(a) and (b). The calculational time was about 1 h. Fig. 2(a) shows that the curves predicted by the 4 schemes coincide well with each other, but M3060 was unstable with more integrations for each time step. Thus, M4080 was selected for the study.

Three time steps of 0.1 s, 1 s, and 2 s were studied. Fig. 3 shows the temperature distributions along the axial direction in the water region for the various time steps. The temperature distributions calculated with time steps of 0.1 s, 1 s and 2 s are consistent, but the 2 s time step was not stable and required more iterations. Therefore, the time step of 1 s was used for the remaining calculations.

3.2.2. Experimental validation

This model was validated by comparing with the experimental results. During the tank cooling, the experiments began with a uniform temperature of 99.5 °C with cooling times of 40 h. The average ambient temperature during the experiment of 26 °C was used in the CFD simulation. Fig. 4 compares the experimental and two-dimensional model results. The stratification during the cooling can be observed from the centerline temperature profile. The predicted temperatures agree with the experimental data even after 40 h of cooling with the internal natural convection. As can be seen in Fig. 4(b), for most of the time, the differences between the predictions and the experimental data are smaller than 2 K. The temperature profiles in Fig. 4(a) shows a larger temperature gradient seen near the bottom while the gradient near the upper side is very small. After cooling for 1 h, the thermal stratification occupies the bottom 0.05 m of the tank with the temperature gradient near the bottom being about 164 °C/m. At 5 h, the thermal stratification extends to 0.08 m from the bottom with the temperature gradient near the bottom being about 143 °C/m. At 15 h, the thermal stratification extends to 0.16 m with the temperature gradient near the bottom being about 88.6 °C/m. The height of the thermal stratification region and the temperature gradient near the bottom do not change much in the next 25 h of cooling.

The maximum temperature difference in the tank shows the thermal stratification increase in the tank more clearly. The predicted and measured maximum temperature differences in the tank changes with time are shown in Fig. 5. The thermal stratification in the storage tank can be divided into the formation process and the degradation process. During the formation process, the thermal stratification in the tank grows quickly during the first 5 h of cooling with the highest thermal stratification at about 10 h of cooling. The maximum temperature difference in the tank is about 7.6 °C. Then, thermal stratification in the tank gradually decreases during the rest of the cooling process with the degradation process being much slower than the formation process.

3.3. Results and discussion

3.3.1. Evolution of the transient natural convection flow

The transient natural convection flow inside the tank is illustrated in Figs. 6 and 7. The cooling process can be divided into the transient regime and quasi-steady regime (Hmouda et al., 2010; Rodríguez et al., 2009). The velocity fields after cooling for 1 min, 3 min, 4 min, and 7 min are shown in Fig. 6 (Velocities with magnitudes smaller than 0.5 mm/s are not shown). When the sidewall is cooled by heat losses to the environment, vertical thermal boundary layers develop very rapidly on the side wall (at 1 min). The cooled fluid near the wall travels down the wall and interacts with the fluid in the core (at 3 min and 4 min). At the same time, convective cells form along the top wall and transport fluid to the core of the tank. The movement of the cold fluid throughout the tank and the cold stream descending on the side wall continues for just a short time with much less motion seen near the bottom of the tank

Table 2
Four types of mesh studied.

MESH Scheme	Radial direction	Axial direction	Insulation	Time step
M3060	Bi-geometric law First row space: 0.001 m; Growth factor: 1.2; Nodes: 30	Bi-geometric law First row space: 0.001 m; Growth factor: 1.2; Nodes: 60	Bi-geometric law Growth factor: 1; Nodes: 5	0.1 s
M4080	Bi-geometric law First row space: 0.001 m; Growth factor: 1.2; Nodes: 40	Bi-geometric law First row space: 0.001 m; Growth factor: 1.2; Nodes: 80	Bi-geometric law Growth factor: 1; Nodes: 5	0.1 s
M50100	Bi-geometric law First row space: 0.001 m; Growth factor: 1.2; Nodes: 50	Bi-geometric law First row space: 0.001 m; Growth factor: 1.2; Nodes: 100	Bi-geometric law Growth factor: 1; Node: 5	0.1 s
M501001	Bi-geometric law First row space: 0.001 m; Growth factor: 1.2; Nodes: 50	Bi-geometric law First row space: 0.001 m; Growth factor: 1.2; Nodes: 100	Bi-geometric law First row space: 0.001 m; Growth factor: 1.2; Nodes: 10	0.1 s

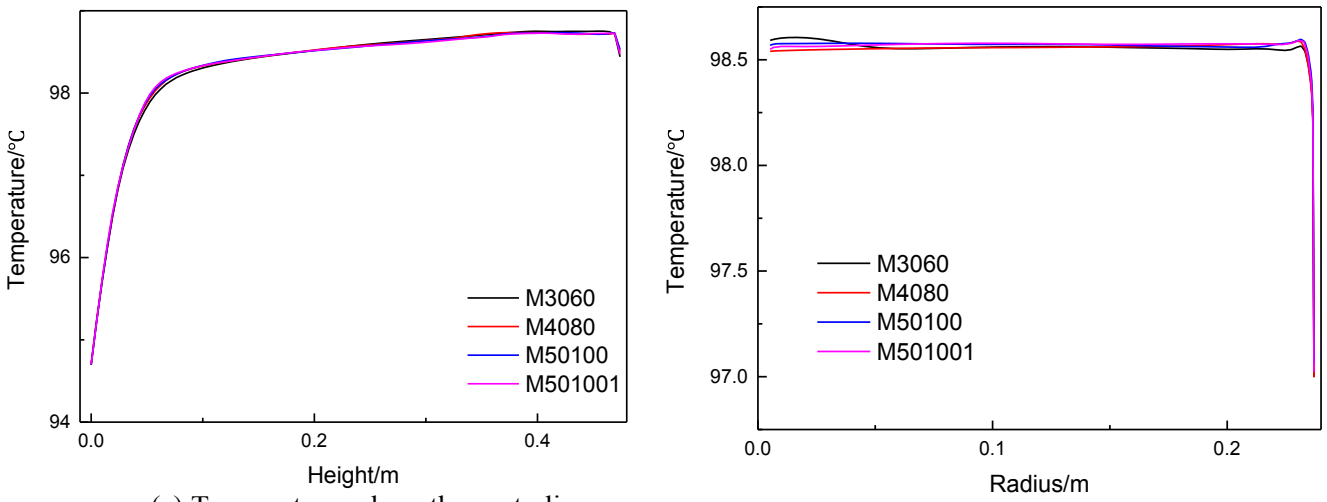

(a) Temperatures along the centerline

(b) Temperatures along the radius 0.257 m above the bottom

Fig. 2. Comparison of the four mesh designs.

after 7 mins.

In this case, most of the cooling is in the quasi-steady regime. In this regime, the convection near the side and top walls is more intense than in other locations in the tank, with very little convection near the bottom (velocities less than 0.5 mm/s) because the temperature of the bottom wall is lower than the water near the wall, so conduction dominates at the bottom. The thermal stratification at the bottom is then mainly caused by conduction. The velocities after cooling for 10 h, 20 h, 30 h, and 40 h are shown in Fig. 7 (velocities smaller than 0.5 mm/s are again neglected).

The natural convection at the top of the tank is caused by heat losses from the top. The velocity field along the upper side shows the mixing process that weakens with time as the cooled water near the top goes down and mixes with the hotter water in the core.

The natural convection near the side wall is caused by the cooling of the side wall. The velocity fields shown in Fig. 7 show the velocity boundary layer near the side wall. This boundary layer works like a channel that transfers the cooled water from the upper part of the tank to the lower part. This channel becomes shorter as the water in the tank cools because cooled water generated at the upper side of the tank is initially much heavier than the hot water near the bottom. Later, as the tank cools, the temperature near the bottom decreases and less cooled water reaches the bottom. The result is that the velocity boundary layer near the side wall becomes shorter as seen in Fig. 7.

3.3.2. *Dimensional analysis*

Dimensional analysis was used to develop a correlation for the tank cooling processes. The results show that conduction is more important at the bottom, so the natural convection at the bottom can be neglected because the bottom wall temperature is lower than the water near the bottom. The conditions along the side and top walls of the storage tank were then analyzed to develop Nusselt number correlations for these surfaces. Previous tank cooling studies have used different definitions of the Grashof Number that are used for natural convection in large regions (Oliveski et al., 2003); therefore, the Nusselt numbers for tank cooling could not be compared for large regions. However, the Nusselt number and Grashof number are defined here in the same way as for large regions. For the tank side wall, the Nusselt number and Grashof number definitions for a vertical plate are used:

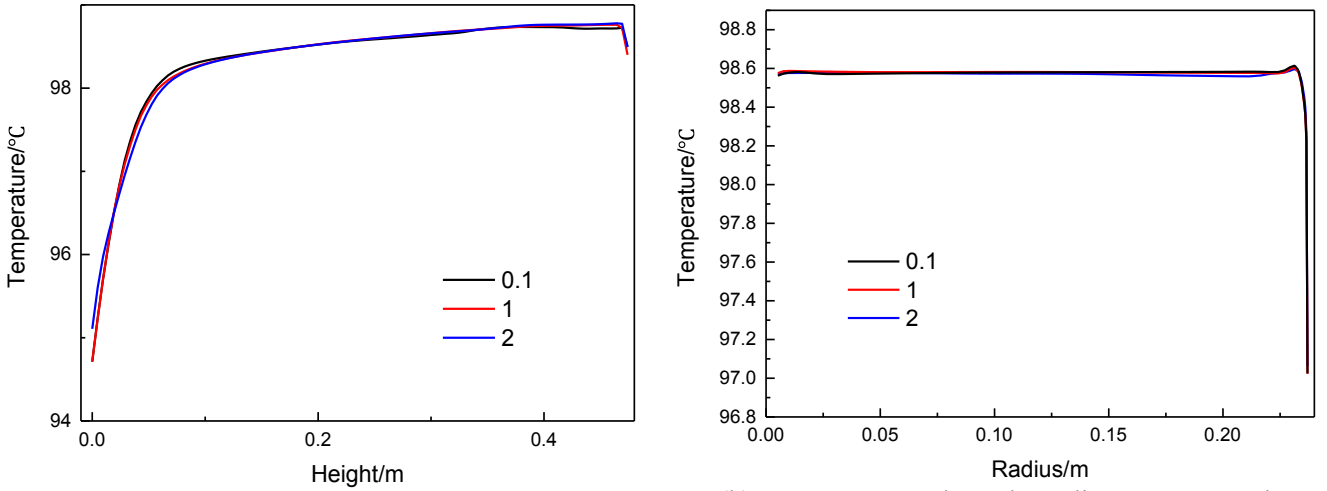

(a) Temperatures along the centerline;

(b) Temperatures along the radius at 0.257 m above the base

Fig. 3. Comparison of the predictions for various time steps.

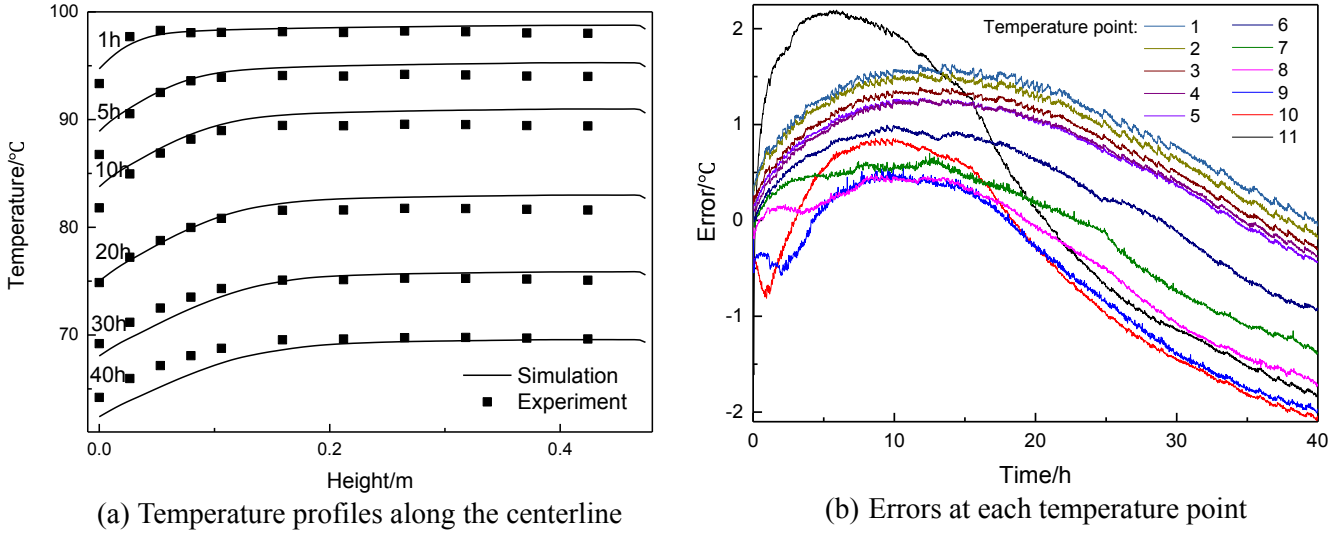

(a) Temperature profiles along the centerline (b) Errors at each temperature point

Fig. 4. Experimental validation of the CFD model.

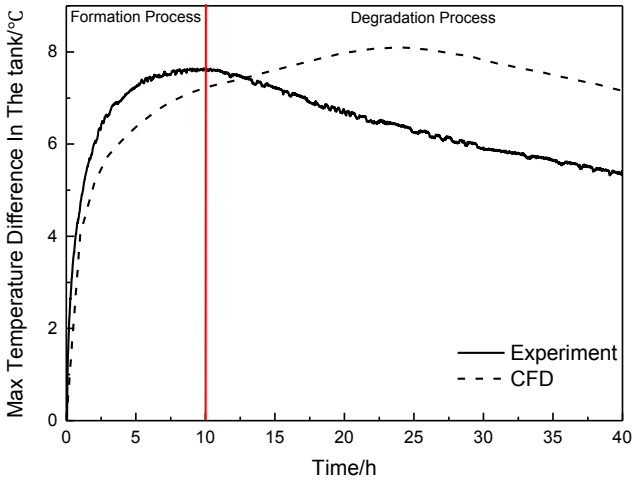

Fig. 5. Maximum temperature difference in the tank.

$$Nu_s = \frac{h_s H}{\lambda};\ Gr_s = \frac{g\beta(\bar{T} - \bar{T}_s)H^3}{\upsilon^2};\ \bar{T} = \frac{4}{\pi D^2 H}\int_0^H \int_0^{D/2} \pi DTdrdz \tag{14}$$

For the top wall, the Nusselt number and Grashof number definitions for a horizontal plate are used:

$$Nu_t = \frac{h_t L}{\lambda};\ Gr_t = \frac{g\beta(T_{\max} - \bar{T}_t)L^3}{\upsilon^2};\ L = \frac{A_t}{P_t} \tag{15}$$

Here, T_{max} is the maximum temperature along the tank centerline. The predicted temperatures along the top and side walls were then fit to develop correlations relating the Nusselt numbers and the Grashof numbers along the top and side walls. For the side wall:

$$Nu = 1.6837(GrPr)^{0.2319},\ 6.3 \times 10^8 < Gr < 1.3 \times 10^{10},\ r = 0.86 \tag{16}$$

For the top wall:

$$Nu = 0.9629(GrPr)^{0.2128},\ 1.3 \times 10^7 < Gr < 1.6 \times 10^8,\ r = 0.88 \tag{17}$$

The correlation coefficients verify the validities of these correlations. The Nusselt numbers for the side and top walls are a little bigger than in a large space for the same Grashof number (Bergman et al., 2011; Shiming Yang, 2006). The two-dimensional model results given

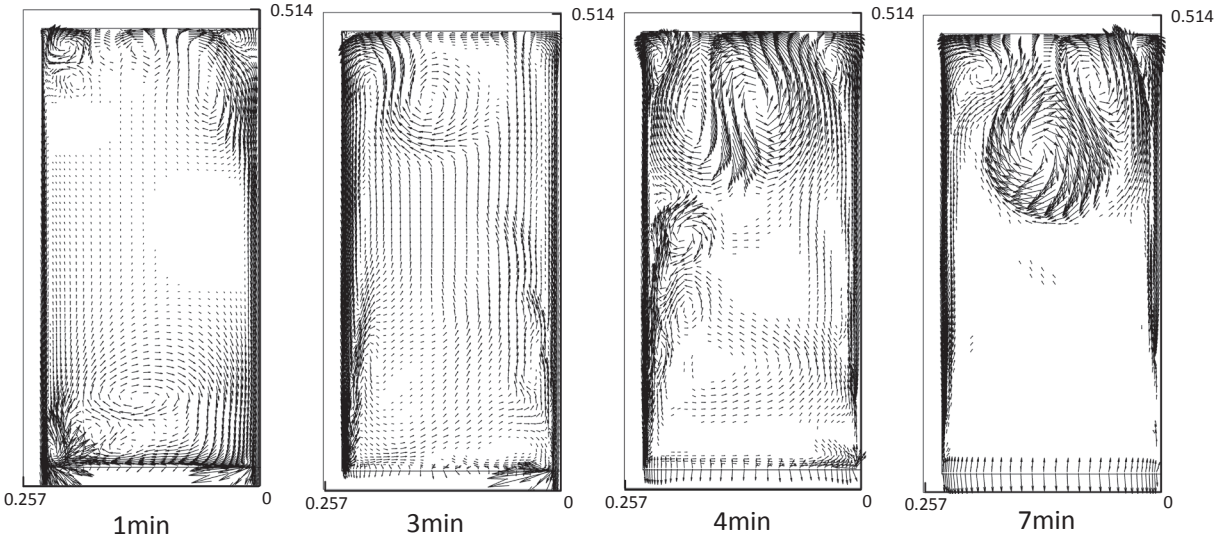

Fig. 6. Velocities in the tank as the natural convection flow initially develops.

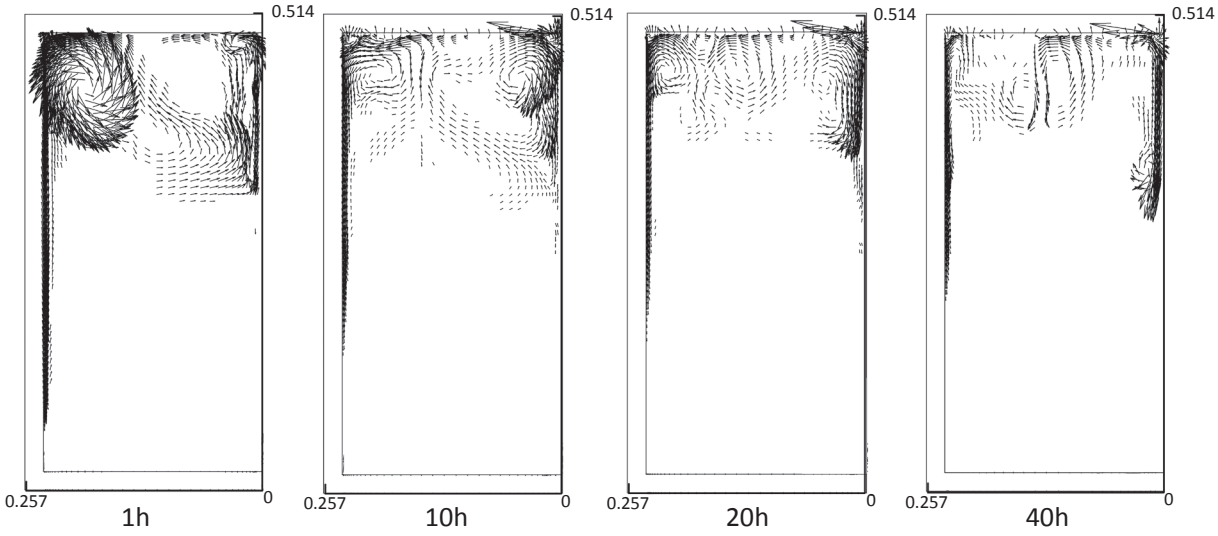

Fig. 7. Velocities in the tank in the quasi-steady regime.

Table 3
Models tested here.

No.	Name	Sources
1	CFD	This study
2	Simple model	–
3	MM	De Césaro Oliveski et al. (2003)
4	MI	De Césaro Oliveski et al. (2003)
5	Fan's model	Fan and Furbo (2012), Fan et al. (2015)
6	Thornton's model	Thornton et al. (2010)

in the previous section can be used to understand the one-dimensional model introduced in the next section.

4. One dimensional model

4.1. Comparison of the one and two-dimensional models

Commercial software products for simulating solar energy heating systems use one-dimensional models, the so-called multimode models, to calculate the thermal behavior of the tank. The tank models are divided into horizontal segments (a simple model) with each segment modeled using

$$Mc_p \frac{\partial T_i}{\partial t} = kA_t \Delta z \frac{d^2 T_i}{dz^2} + U_s A(T_i - T_{env}) \tag{18}$$

Natural convection is not considered in such simple models, so thermal inversion can occur. De Césaro Oliveski et al. (2003) showed that the multinode with mean (MM) and multinode with inverse (MI) models gave reasonable temperature distributions in the tank. The type 534 model by Thornton et al. (2010) in the Tess Library for TRNSYS used a model similar to MM. The MM and MI models can predict the heat losses in the tank because both models both model the mixing near the top. The MM model mixes the cooled water generated from the top wall with the hot water near the wall using the mean temperature among the segments involved in the thermal inversion. The MI mode realizes this mixing process by interchanging the temperatures of the segments involved in the inversion.

Natural convection in the tank is caused by the heat loss from top and side walls. However, the MM and MI models only analyze the natural convection near the top wall. Therefore, these one-dimensional models are not complete. The two-dimensional analysis shows that the velocity boundary layer along the side wall works like a channel to transfer cooled water from the upper part of the tank to the lower part. Along the upper side of the tank, cooled water flows down and the heat loss along the upper side seems to be less than the heat transfer at that element, $U_s A(T_i - T_{env})$. Along the lower side of the tank, the cooled water from the boundary layer channel mixes with the water along the lower side of the tank, so the heat loss along the lower side seems to be more than $U_s A(T_i - T_{env})$. Thus, the flow makes the heat loss coefficients along the tank wall look like they are not the same as expected.

Fan and his colleagues develop a model to predict the temperature distribution in a storage tank during the heat loss process based on CFD simulation results (Fan and Furbo, 2012; Fan et al., 2015). Their model considered the natural convection along both the top and side walls.

Numerical tests were conducted to study the results of the 6 models listed in Table 3. The validated two-dimensional model results are used as the reference. The tests modeled a water storage tank with a height to diameter ratio of 1:1 and a height of 0.474 m. The top and bottom of the tank were adiabatic to study the thermal stratification caused by the heat loss from the side wall with a heat loss coefficient along the side wall of 6 W/m^2/K. The tank was cooled from a 99.5 °C for 10 h with an ambient temperature of 26 °C. The geometric parameters and boundary conditions are shown in Fig. 8.

There is no perfect insulation for storage tanks (Oliveski et al., 2005) and the adiabatic boundary conditions used here for the top and bottom are just a test to show the limitations of these models. Also, previous simulations of this type of cooling have shown clear thermal

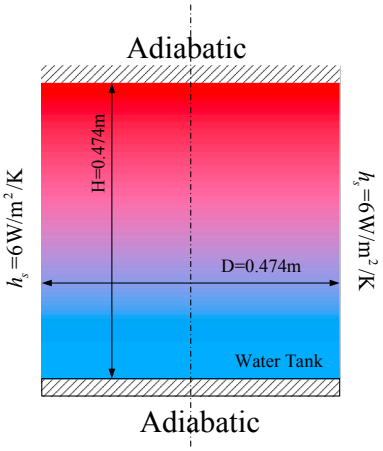

Fig. 8. Geometric parameters and boundary conditions for the model comparisons.

stratification (Karatas and Derbentli, 2017; Lin and Armfield, 1999; Oliveski et al., 2005; Papanicolaou and Belessiotis, 2002). In these numerical tests, the thermal stratification is only caused by heat loss from the side wall. As can be seen in Fig. 9, the thermal stratification caused by natural convection near the side wall is not considered in the MM, MI and Thornton models; thus, no temperature gradient develops with these methods and their centerline temperature profiles are uniform as shown in Fig. 9. Fan's model gives some thermal stratification in the tank, but the temperature gradient is much less than that from the CFD model.

4.2. Augmented computational model

The MM and MI models can simulate the mixing near the top, but the natural convection near the side is also important. The natural convection near the side wall transfers cooled water from the upper side region down to the lower side region. Thus, the heat transport is caused by mass transport. The two-dimensional model results show that the velocities during cooling are quite small; thus, the mass transport can be simplified to a heat transfer model.

This augmented model includes the natural convection effect near the side wall. As shown in Fig. 10, the storage tank is divided into n segments with each segment characterized by a bulk temperature and a cooled water temperature. In the MM, MI and simple models, the heat losses from the side walls for each segment are calculated based on the temperature of that segment, $U_sA(T_i - T_{amb})$. However, this is not correct due to the natural convection along the side wall that carries some of the heat down the tank wall as the cooled water generated near the side wall flows down the tank through the boundary layer driven by buoyancy. The cooled water will not stop until it reaches a segment with the same temperature. The model assumes that the cooled water is evenly divided into the segments that it passes through in a simple computational model to simulate the natural convection near the side wall. The temperature of the cooled water in the boundary layer can be estimated as:

$$T_{c,i} \approx \frac{T_{w,i} + T_i}{2} \tag{19}$$

When $T_k \geqslant T_{c,i}$ and $T_{k+1} < T_{c,i}$, the cooled water from the ith segment will stop at the kth segment whose density is equal to that of the cooled water in the ith segment. The heat loss from the ith segment is carried down by the cooled water and is evenly divided into the segments from i to k as $-\frac{U_sA(T_i - T_{amb})}{k-i+1}$, as shown in Fig. 10.

Then, the energy balance equation for segment i can be written as:

$$Mc_p\frac{\partial T_i}{\partial t} = kA_t\Delta z\frac{d^2T_i}{dz^2} + U_sA\sum_{j=1}^{i}(T_j - T_{env})f_j;\ f_j = \frac{1}{k-j+1}(T_k \geqslant T_{c,j},\ T_{k+1} < T_{c,j}) \tag{20}$$

In this model, the heat loss from the side wall is not $U_sA(T_i - T_{amb})$ but is $U_sA\sum_{j=1}^{i}(T_j - T_{amb})f_j$ due to the influence of the natural convection. The energy balance at the wall gives the cooled water temperature in the boundary layer as:

$$T_{c,i} \approx \frac{U_s(T_{env} - T_i)}{2h} + T_i \tag{21}$$

4.3. Model study and validation

4.3.1. Natural convection coefficient

The natural convection coefficient in the water along the side wall, h, is an important parameter for the model; thus, the various natural convection correlations listed in Table 4 were studied here.

The natural convection coefficient on the water side is about 300 W/m^2/K in most cases, so constant natural convection coefficients of 200, 300 and 400 W/m^2/K were also tested. Neglecting the natural convection along the side wall (setting $h = \infty$) gives the same result as the MM model. Thus, the MM model is a simplified case of this model. The flow chart for this model is shown in Fig. 11.

The numerical test done in Section 4.1 was used to evaluate this model with the various natural convection coefficients with the predicted temperature profiles shown in Fig. 12.

As can be seen in Fig. 12, the temperature distributions predicted by this model are very close to the results from the CFD simulation. A higher natural convection coefficient will result in less thermal stratification. When the natural convection coefficient is infinite (1×10^{10}), this method is the same as the MM method with no thermal stratification. Thus, this model can reasonably approximate the natural convection effect near the side wall. The temperatures predicted using the natural convection coefficients from the first three models in Table 4 all agree well with the CFD results with differences of less than 0.5 °C. The natural convection coefficient given by Bergman et al. (2011) give the smallest differences from the CFD result, so this correlation was used in the following study.

4.3.2. Experimental validation

The experiment used to validate the two-dimensional model is also used here to validate this model. The heat loss coefficient from the tank was calculated as:

$$U = \frac{1}{\frac{1}{h_{env}} + \frac{\delta}{\lambda_{ins}}} \tag{22}$$

As shown in Fig. 13(a) and (b), the temperature profiles predicted by this model agree well with the experimental data with most of the temperature differences between this model and the data being less than 2 °C. Thus, this model can accurately predict the thermal stratification in a water storage tank during cooling.

This model gives a clear understanding of the thermal stratification process in a cylindrical tank. During most of the cooling, the thermal stratification is caused by three different mechanisms. First, the heat loss from the bottom cools the water near the bottom which increases the thermal stratification near the bottom. Conduction heat transfer is important in this process. Second, the cooled water generated near the top of the tank mixes with warmer water near the top so no inverse temperature gradient develops near the top during the cooling. Models must consider both of these influences on the thermal stratification to give acceptable temperature stratification in the tank. The third and most mentioned process is the natural convection near the side wall. The heat loss from the side creates a boundary layer near the side that transfers cooled water from the upper part down to the lower part

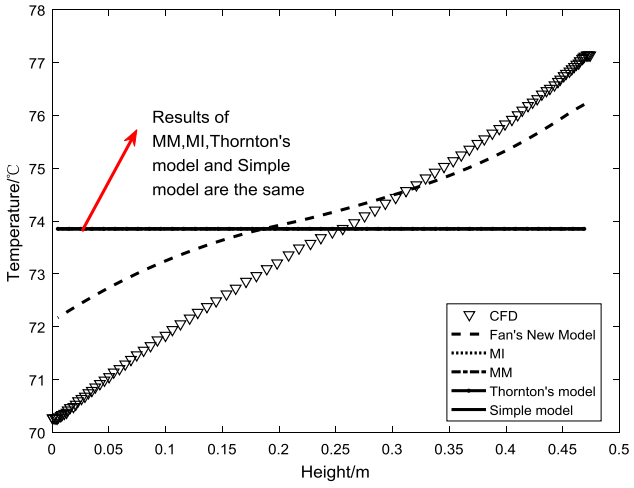

Fig. 9. Predicted temperature profiles after cooling for 10 h.

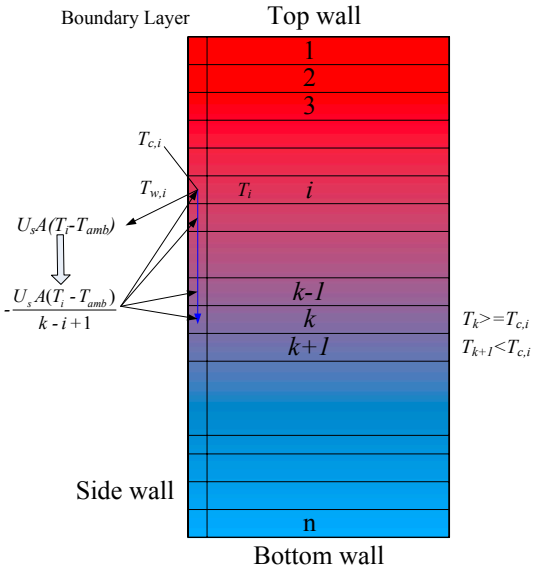

Fig. 10. Augmented computational model.

Table 4
Natural convection coefficients along the side wall.

No.	Sources	Correlations
1	Heat Transfer (Yang and Tao, 2006)	$1.43\times10^4 < Gr < 3\times10^9$: $h=\frac{\lambda}{H}0.59(Gr\,Pr)^{0.25}$ $3\times10^9 < Gr < 2\times10^{10}$: $h=\frac{\lambda}{H}0.0292(Gr\,Pr)^{0.39}$ $2\times10^{10} < Gr$: $h=\frac{\lambda}{H}0.11(Gr\,Pr)^{1/3}$
2	Fundamentals of Heat and Mass Transfer (Bergman et al., 2011)	$h=\frac{\lambda}{H}\left\{0.825+\frac{0.387(GrPr)^{1/6}}{[1+(0.492/Pr)^{9/16}]^{8/27}}\right\}^2$
3	This study	$h=\frac{\lambda}{H}1.6837(Gr\,Pr)^{0.2319}$
4	Constant	$h=200/300/400$
5	Infinity	$h=10^{10}$

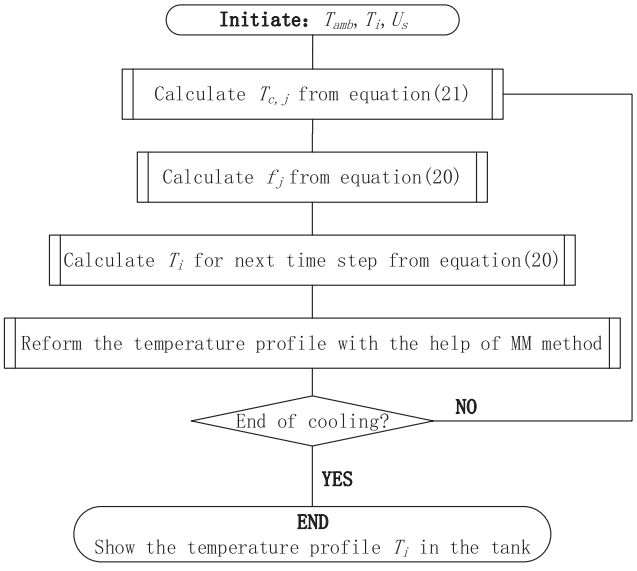

Fig. 11. Model flow chart.

which creates the thermal stratification. This model includes the conduction near the bottom by the one-dimensional heat conduction through the segments. Natural convection near the top is realized by the use of the mean temperature among the segments involved in the thermal inversion. Natural convection near the side is realized by the model including the heat transport in the boundary layer.

4.4. Application and comparative study

The height-to-diameter ratio of a cylindrical tank is a significant factor influencing the thermal stratification. Most comparisons of tanks with different height to diameter ratios have been based on charging and discharging models (Yaïci et al., 2013). Past experiments and numerical simulations of the charging and discharging processes of hot water storage tanks have shown that good stratification develops when the tank aspect ratio was 2–4 (Bouhdjar and Harhad, 2002; Haller et al., 2009; Park et al., 2013). However, there are few studies comparing the effect of the height to diameter ratio on the cooling of tanks in standby mode. Park et al. studied the effect of aspect ratio on the thermal stratification and heat loss of torus-shaped rock caverns for underground thermal energy storage (Park et al., 2013). Yang et al. studied the heat loss of tanks with various shapes (Yang et al., 2016).

The cooling of tanks with height to diameter ratios of 10:1, 5:1, 1:1, 1:5 and 1:10 is studied here using the current model. All of the water tanks were designed with the same volume of 83.6 L as shown in Table 5. The tanks were made of stainless steel 304 with 1 mm thick walls and 20 mm thick glass wool insulation layers. The water in the tanks was initially static with a uniform temperature of 99.5 °C. The ambient temperatures were all 26 °C.

4.4.1. Thermal energy storage capacity

The thermal energy storage efficiency is defined as the ratio of the thermal energy stored in a water tank at a given time to the initial thermal energy stored in the tank.

$$\eta_1 = \frac{E - E_{env}}{E_{ini} - E_{env}} \tag{23}$$

where E is the internal energy in the water tank (kJ) calculated as:

$$E = \int_V \rho e dV \tag{24}$$

The thermal exergy storage efficiency is defined as the ratio of the thermal exergy stored in the water tank at a given time to the initial thermal exergy stored in the tank.

$$\eta_2 = \frac{Ex - Ex_{env}}{Ex_{ini} - Ex_{env}} \tag{25}$$

$$Ex = \int_V \rho ex dV \tag{26}$$

The exergy was calculated based on a base temperature of T_{env} = 25 °C and a pressure of p_{env} = 0.101325 MPa.

The tank with the smallest height to diameter ratio 1:1 has the smallest surface area and the smallest heat loss. Thus, as shown in Fig. 14(a) and (b), the energy and exergy efficiencies of the tank with H/D = 1:1 are the highest. The tank with H/D = 1:10 has the largest surface area and the lowest energy and exergy efficiencies. The tank with H/D = 1:1 also has the biggest storage capacity of all these cases.

4.4.2. Entropy generation

The entropy generation during cooling of a storage tank is (Biswal and Basak, 2017; Chang et al., 2016; Hoffmann et al., 2017):

$$\dot{S}_{gen} = \frac{dS_{gen}}{dt};\ S_{gen} = -\rho c_p \int \ln\left(\frac{T}{T_0}\right) dV \tag{28}$$

Entropy generation minimization is an important tool for optimizing thermal systems by minimizing the irreversibility measured by the entropy generation. During cooling, the entropy production is mainly caused by the entropy changes due to heat losses. The tank with H/D = 1:1 has the smallest heat loss, so it also has the smallest entropy

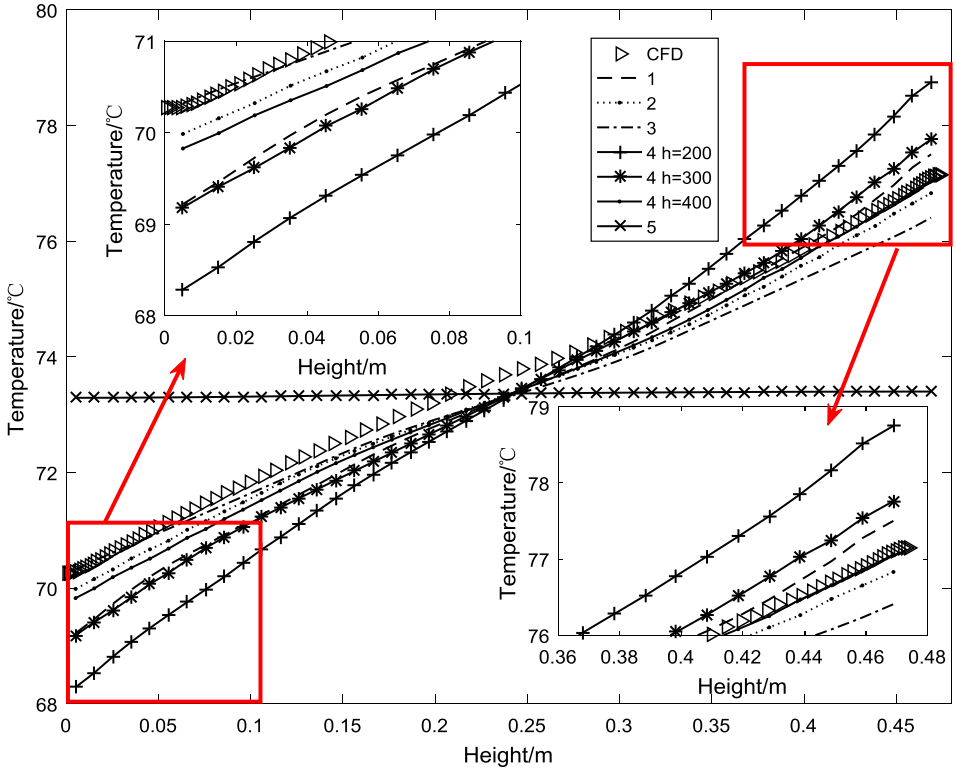

Fig. 12. Predictions of the model with the various natural convection coefficients.

generation during cooling, as shown in Fig. 15(a). The entropy generation during cooling cannot show the thermal stratification in the cylindrical tank seen by the heat loss analysis. As can be seen in Fig. 15(b), as the tank cools, the water temperature decreases and the entropy generation rate slows.

4.4.3. Maximum temperature difference in the tank

The tank shape significantly affects the degree of thermal stratification in a cylindrical tank. This phenomenon is illustrated in 0 which shows the maximum temperature differences for all the water tank shapes, $\Delta T_{max} = T_{max} - T_{min}$, over time. These differences reflect the variation of the thermal stratification over time. As seen in Fig. 16, increasing the aspect ratio increases the thermal stratification in the cylindrical tank. The thermal stratification in the tanks with H/D = 5:1 and H/D = 10:1 are almost the same.

Table 5
Water tank models.

H/D	Height/m	Diameter/m	Heat transfer surface area/m^2
1:10	0.102	1.021	1.966
1:5	0.162	0.811	1.445
1:1	0.474	0.474	1.059
5:1	1.386	0.277	1.328
10:1	2.200	0.220	1.597

The maximum temperature differences during the whole cooling process are shown in Fig. 17. For H/D < 3, H/D greatly influences the thermal stratification with higher aspect ratios leading to greater

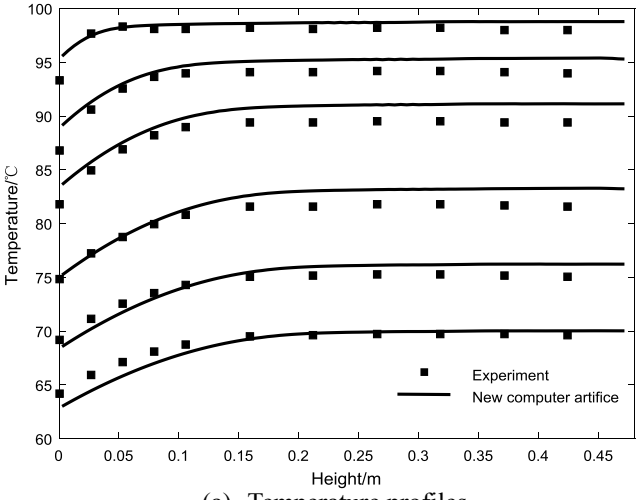

(a) Temperature profiles

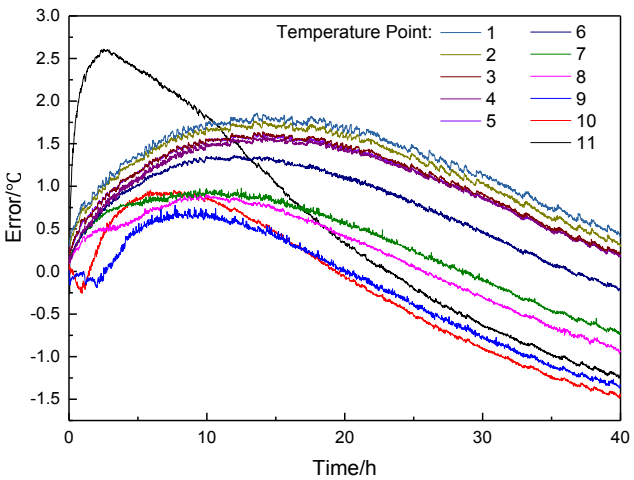

(b) Errors with the model

Fig. 13. Experimental validation of the computational model.

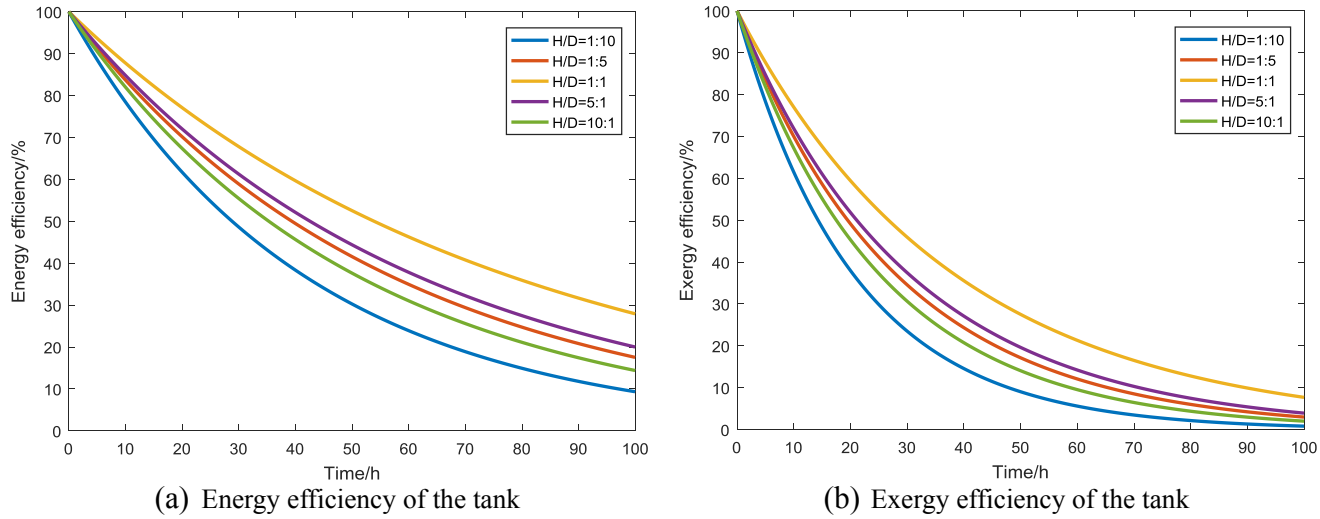

Fig. 14. Influence of aspect ratio on the thermal energy storage capacity.

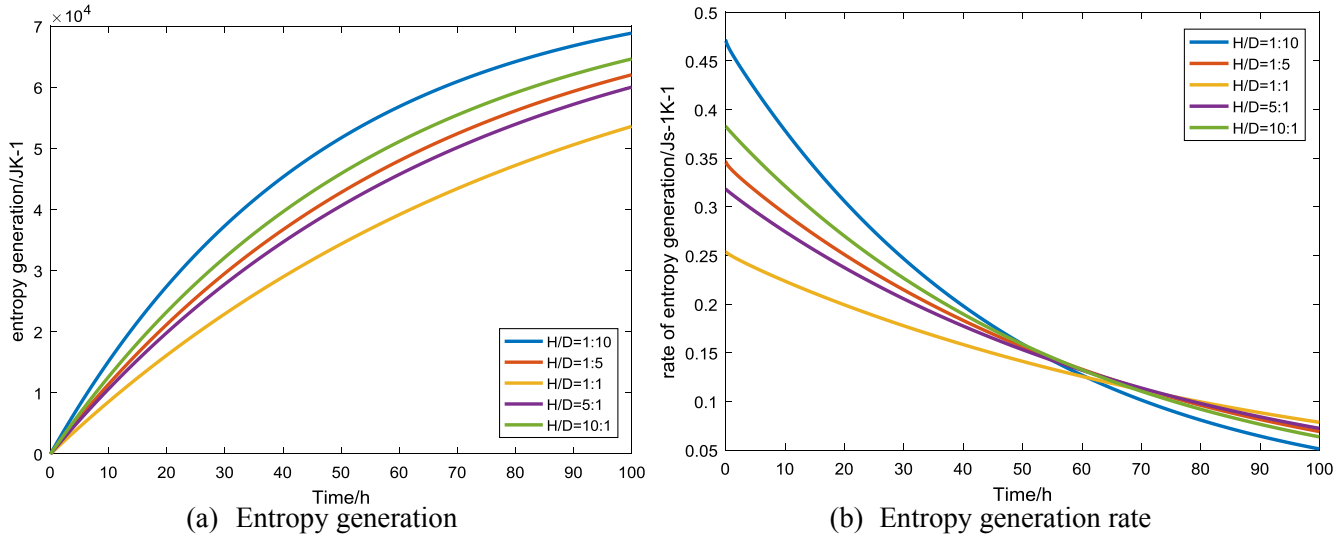

Fig. 15. Entropy generation during tank cooling.

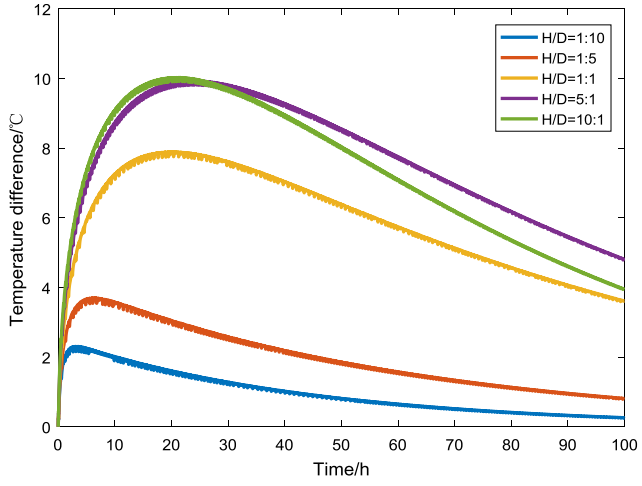

Fig. 16. Influence of H/D on the maximum temperature difference in a tank.

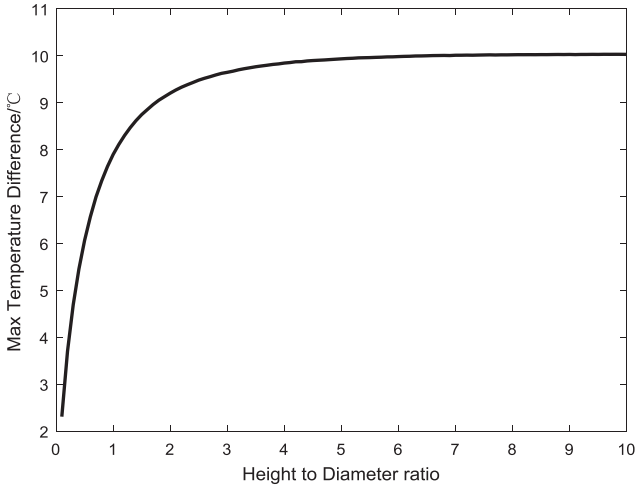

Fig. 17. Maximum temperature difference during cooling.

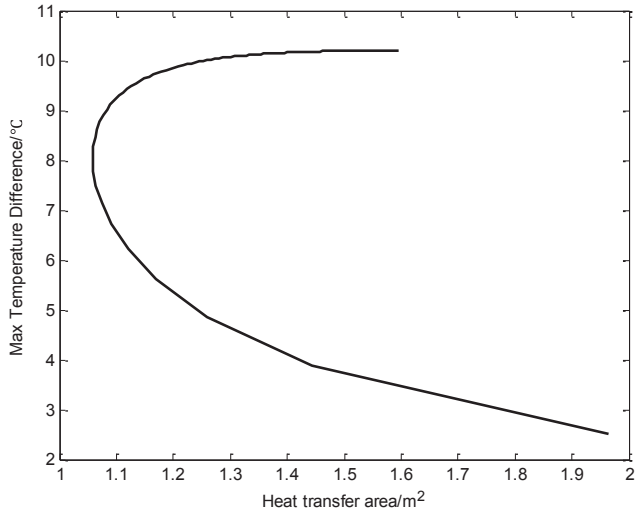

Fig. 18. Influence of the heat transfer area.

stratification. For H/D > 3, the aspect ratio has little influence on the thermal stratification.

The tank heat transfer area also influences the maximum temperature difference with ΔT_{max} decreasing with increasing heat transfer area for H/D < 1 and ΔT_{max} increasing with increasing heat transfer area for H/D > 1 as shown in Fig. 18.

5. Conclusions

The cooling of a large water tank used to store heat for later use was studied experimentally and numerically. A two-dimensional CFD model was validated against the experiment data and then used to study the thermal stratification mechanisms during cooling. The cooling process can be divided into a first short stage of about 4 min in this study with natural convection throughout the entire tank and a second stage with natural convection mainly located near the side and top walls. The heat transfer along the bottom of the tank during the second state was dominated by conduction. The Nusselt numbers along the side and top walls were modeled by fitting the numerical results using correlations similar to those used for natural convection in large spaces. The Nusselt number for the side wall of the tank was $Nu = 1.6837(GrPr)^{0.2319}$ and for the top of the tank was $Nu = 0.9629(GrPr)^{0.2128}$. The two-dimensional study of the thermal stratification mechanisms was then used to develop a one-dimensional model that was validated against the experimental results. Most of the time, the temperature differences between the one-dimensional model and the experimental data were smaller than 2 °C. Then, the model was used to analyze the tank temperatures for height to diameter ratios of 1:10, 1:5, 1:1, 5:1 and 10:1. The tank with a height to diameter ratio of 1:1 has the highest energy efficiency, the highest exergy efficiency, and lowest entropy generation during the cooling process. Further analyses shows that when H/D < 3, increasing the H/D leads to more thermal stratification, while for H/D > 3, the aspect ratio has little influence on the thermal stratification.

Acknowledgments

Supported by Strategic science and technology project of the Chinese Academy of Sciences (No. XDA21050200) and Guangdong Innovative and Entrepreneurial Research Team Program (No. 2013N070).

References

Alizadeh, S., 1999. An experimental and numerical study of thermal stratification in a horizontal cylindrical solar storage tank. Sol. Energy 66 (6), 409–421.
Avallone, E., Cunha, D.G., Padilha, A., Scalon, V.L., 2016. Electronic multiplex system using the Arduino platform to control and record the data of the temperatures profiles in heat storage tank for solar collector. Int. J. Energy Environ. Eng. 7 (4), 391–398.
Baeten, B., Confrey, T., Pecceu, S., Rogiers, F., Helsen, L., 2016. A validated model for mixing and buoyancy in stratified hot water storage tanks for use in building energy simulations. Appl. Energy 172, 217–229.
Bergman, T.L., Incropera, F.P., DeWitt, D.P., Lavine, A.S., 2011. Fundamentals of Heat and Mass Transfer. John Wiley & Sons.
Biswal, P., Basak, T., 2017. Entropy generation vs energy efficiency for natural convection based energy flow in enclosures and various applications: a review. Renew. Sustain. Energy Rev. 80, 1412–1457.
Bouhal, T., Fertahi, S., Agrouaz, Y., El Rhafiki, T., Kousksou, T., Jamil, A., 2017. Numerical modeling and optimization of thermal stratification in solar hot water storage tanks for domestic applications: CFD study. Sol. Energy 157, 441–455.
Bouhdjar, A., Harhad, A., 2002. Numerical analysis of transient mixed convection flow in storage tank: influence of fluid properties and aspect ratios on stratification. Renew. Energy 25 (4), 555–567.
Cabelli, A., 1977. Storage tanks—a numerical experiment. Sol. Energy 19 (1), 45–54.
Castell, A., Medrano, M., Solé, C., Cabeza, L.F., 2010. Dimensionless numbers used to characterize stratification in water tanks for discharging at low flow rates. Renew. Energy 35 (10), 2192–2199.
Chang, C., Wu, Z., Navarro, H., Li, C., Leng, G., Li, X., Yang, M., Wang, Z., Ding, Y., 2017. Comparative study of the transient natural convection in an underground water pit thermal storage. Appl. Energy 208, 1162–1173.
Chang, Z., Li, X., Xu, C., Chang, C., Wang, Z., Zhang, Q., Liao, Z., Li, Q., 2016. The effect of the physical boundary conditions on the thermal performance of molten salt thermocline tank. Renew. Energy 96, 190–202.
Cruickshank, C.A., Harrison, S.J., 2010. Heat loss characteristics for a typical solar domestic hot water storage. Energy Build. 42 (10), 1703–1710.
De Césaro Oliveski, R., 2013. Correlation for the cooling process of vertical storage tanks under natural convection for high Prandtl number. Int. J. Heat Mass Transf. 57 (1), 292–298.
De Césaro Oliveski, R., Krenzinger, A., Vielmo, H.A., 2003. Comparison between models for the simulation of hot water storage tanks. Sol. Energy 75 (2), 121–134.
Erdemir, D., Altuntop, N., 2016. Improved thermal stratification with obstacles placed inside the vertical mantled hot water tanks. Appl. Therm. Eng. 100, 20–29.
Fan, J., Furbo, S., 2012. Buoyancy driven flow in a hot water tank due to standby heat loss. Sol. Energy 86 (11), 3438–3449.
Fan, J., Furbo, S., Yue, H., 2015. Development of a hot water tank simulation program with improved prediction of thermal stratification in the tank. Energy Proc. 70, 193–202.
Franke, R., 1997. Object-oriented modeling of solar heating systems. Sol. Energy 60 (3–4), 171–180.
Haller, M.Y., Cruickshank, C.A., Streicher, W., Harrison, S.J., Andersen, E., Furbo, S., 2009. Methods to determine stratification efficiency of thermal energy storage processes – review and theoretical comparison. Sol. Energy 83 (10), 1847–1860.
Hmouda, I., Rodriguez, I., Bouden, C., Oliva, A., 2010. Unsteady natural convection cooling of a water storage tank with an internal gas flue. Int. J. Therm. Sci. 49 (1), 36–47.
Hoffmann, J.F., Fasquelle, T., Goetz, V., Py, X., 2017. Experimental and numerical investigation of a thermocline thermal energy storage tank. Appl. Therm. Eng. 114, 896–904.
Thornton, J.W., D.E.B., McDowell, T.P., 2010. TESS Libs 17 - Component Libraries for the TRNSYS Simulation Environment. University of Wisconsin, S.E.L. (Ed.).
Karatas, H., Derbentli, T., 2017. Natural convection in rectangular cavities with one active vertical wall. Int. J. Heat Mass Transf. 105, 305–315.
Klein, S.A., 1988. TRNSYS-A transient system simulation program, in: Wisconsin-Madison, U.o. (Ed.) Engineering Experiment Station Report, pp. 38–12.
Kurşun, B., 2018. Thermal stratification enhancement in cylindrical and rectangular hot water tanks with truncated cone and pyramid shaped insulation geometry. Sol. Energy 169, 512–525.
Kurşun, B., Ökten, K., 2018. Effect of rectangular hot water tank position and aspect ratio on thermal stratification enhancement. Renew. Energy 116, 639–646.
Lin, W., Armfield, S., 1999. Direct simulation of natural convection cooling in a vertical circular cylinder. Int. J. Heat Mass Transf. 42 (22), 4117–4130.
Oliveski, R.D.C., Krenzinger, A., Vielmo, H.A., 2003. Cooling of cylindrical vertical tanks submitted to natural internal convection. Int. J. Heat Mass Transf. 46 (11), 2015–2026.
Oliveski, R.D.C., Macagnan, M.H., Copetti, J.B., Petroll, A.d.L.M., 2005. Natural convection in a tank of oil: experimental validation of a numerical code with prescribed boundary condition. Exp. Therm. Fluid Sci. 29 (6), 671–680.
Padilha, A., 1983. Estocagem por estratificação térmica de líquido em reservatório.
Papanicolaou, E., Belessiotis, V., 2002. Transient natural convection in a cylindrical enclosure at high Rayleigh numbers. Int. J. Heat Mass Transf. 45 (7), 1425–1444.
Park, D., Kim, H.-M., Ryu, D.-W., Choi, B.-H., Sunwoo, C., Han, K.-C., 2013. The effect of aspect ratio on the thermal stratification and heat loss in rock caverns for underground thermal energy storage. Int. J. Rock Mech. Min. Sci. 64, 201–209.
Powell, K.M., Edgar, T.F., 2013. An adaptive-grid model for dynamic simulation of thermocline thermal energy storage systems. Energy Convers. Manage. 76, 865–873.
Rodríguez, I., Castro, J., Pérez-Segarra, C.D., Oliva, A., 2009. Unsteady numerical simulation of the cooling process of vertical storage tanks under laminar natural convection. Int. J. Therm. Sci. 48 (4), 708–721.
Shiming Yang, W.T., 2006. Heat Transfer, 4th ed. Higher Education Press.
Wang, Z., Zhang, H., Dou, B., Huang, H., Wu, W., Wang, Z., 2017a. Experimental and numerical research of thermal stratification with a novel inlet in a dynamic hot water storage tank. Renew. Energy 111, 353–371.

Wang, Z., Zhang, H., Dou, B., Huang, H., Zhang, G., 2017b. The thermal stratification characteristics affected by a novel equalizer in a dynamic hot water storage tank. Appl. Therm. Eng. 126, 1006–1016.
Yaïci, W., Ghorab, M., Entchev, E., Hayden, S., 2013. Three-dimensional unsteady CFD simulations of a thermal storage tank performance for optimum design. Appl. Therm. Eng. 60 (1–2), 152–163.
Yang, S., Tao, W., 2006. Heat Transfer (4th ed.).
Yang, Z., Chen, H., Wang, L., Sheng, Y., Wang, Y., 2016. Comparative study of the influences of different water tank shapes on thermal energy storage capacity and thermal stratification. Renew. Energy 85, 31–44.
Zhang, H., Baeyens, J., Cáceres, G., Degrève, J., Lv, Y., 2016. Thermal energy storage: recent developments and practical aspects. Prog. Energy Combust. Sci. 53, 1–40.